Towards a full-reference, information-theoretic quality assessment method for X-ray images

Towards a full-reference, information-theoretic quality assessment method for X-ray images

Chrysi Papalazarou[a], Rudolph M. Snoeren[b] Frans M.J. Willems[a], Peter H.N. de With[a,c] , Han Kroon[b] and Peter Rongen[b]

[a]Univ. of Technol. Eindhoven, The Netherlands
[b]Philips Medical Systems, Best, The Netherlands
[c]LogicaCMG, Eindhoven, The Netherlands

ABSTRACT

This work aims at defining an information-theoretic quality assessment technique for cardiovascular X-ray images, using a full-reference scheme (relying on averaging a sequence to obtain a noiseless reference). With the growth of advanced signal processing in medical imaging, such an approach will enable objective comparisons of the quality of processed images. A concept for describing the quality of an image is to express it in terms of its information capacity. Shannon has derived this capacity for noisy channel coding. However, for X-ray images, the noise is signal-dependent and non-additive, so that Shannon's theorem is not directly applicable. To overcome this complication, we exploit the fact that any invertible mapping on a signal does not change its information content. We show that it is possible to transform the images in such a way that the Shannon theorem can be applied. A general method for calculating such a transformation is used, given a known relation between signal mean and noise standard deviation. After making the noise signal-independent, it is possible to assess the information content of an image and to calculate an overall quality metric (e.g. information capacity) which includes the effects of sharpness, contrast and noise. We have applied this method on phantom images under different acquisition conditions and computed the information capacity for those images. We aim to show that the results of this assessment are consistent with variations in noise, contrast and sharpness, introduced by system settings and image processing.

Keywords: Image quality assessment, X-ray imaging, signal-dependent noise, Shannon capacity
SPIE Keyword codes: : DX (digital X-ray), METR (measurement methods), CAR (cardiac imaging), ALG (algorithms)

1. INTRODUCTION

Medical imaging is a highly task-oriented discipline in which image quality (IQ) is effectively judged by the amount of diagnostic information conveyed to the physician. It is therefore interesting to view the image as a carrier of visual information and the imaging system as a communication channel that distorts the message (the anatomical structure of interest) communicated to the receiver (viewer). Information theory provides a framework for the description of information transfer in such a system.

The goal of this work is to perform quality assessment of X-ray images using an information-theoretic framework and to develop a Figure of Merit (FOM) for an objective description of image quality. Our analysis follows a full-reference scheme, in the sense that a noiseless version (reference) of the image to be assessed is assumed to be available. This FOM can then be used to assess the effect of various system settings on the resulting image quality, and also to objectively evaluate the performance of the involved image-processing algorithms.

The paper is organized as follows: in Section 2 some previous attempts to use this framework are mentioned. The proposed method for this assessment is presented in Section 3. Section 4 describes the implementation of the method and a number of measurements performed in a real X-ray system, the Allura Xper FD20*. Finally, the results of the assessment for a number of phantom images are presented in Section 5 and conclusions are drawn in Section 6.

Send correspondence to Chrysi Papalazarou: c.papalazarou@tue.nl
*This system is commercially available by Philips Medical Systems.

2. RELATED WORK

Information theory as an approach in image analysis and processing has been applied in several contexts, such as noise filtering (see for example Awate and Whitaker[1]) and image registration (a thorough overview is given by Pluim *et al.*[2]). In the field of quality assessment, there has been significant work in the past decades to apply Shannon's theory to two-dimensional signals, and derive expressions for the information capacity of imaging systems. Huck *et al.*[3] made an extensive analysis of imaging systems as information carriers, distinguishing between the stages of image gathering, encoding, restoration and display, following the assumption of independent Gaussian noise. Wagner *et al.*[4] applied Shannon's noisy channel coding theorem in CT, expressing the information capacity in terms of the MTF and NPS. Similar work has been done by Fuderer[5] for the case of MR images. Such an information-theoretic fidelity criterion has also been applied by Sheikh *et al.*[6] in the wavelet domain, on natural images, incorporating a human observer model. In all the aforementioned work, the noise was assumed signal-independent, in compliance with Shannon's theorem. The present work aims to extend this description for signal-dependent noise, as is the case in radiography, and also to examine the effect of image processing on information content.

3. PROPOSED METHOD OF IQ ASSESSMENT

In the following, first we will give a brief explanation of basic concepts of information theory and demonstrate how it can be applied to imaging. Second, the complications for this approach introduced by the nature of noise in radiographic images are explained and a solution is proposed which allows information theoretic IQ assessment for this type of images.

3.1 Information theory concepts in 2-D

The work of Shannon[7] has provided a framework for the assessment of digital communication. The Shannon entropy, as a description of the amount of uncertainty or surprise contained in a signal, can be expressed in terms of the underlying distribution $p(x_i)$ of the random variable X by:

$$H(X) = -\sum_{i=1}^{n} p(x_i) \cdot \log(p(x_i)), \tag{1}$$

where n is the number of states that the (discrete) signal can assume. In the context of our full-reference scheme, an important concept is the Mutual Information (MI) between an input distribution X and an output Y, which describes the amount of information Y conveys about X:

$$MI(X;Y) = H(X) + H(Y) - H(X,Y) = H(Y) - H(Y|X) = \sum_{X,Y} p(x,y) \log_2 \frac{p(x,y)}{p(x) \cdot p(y)}. \tag{2}$$

In terms of imaging, this variable can be regarded as the extent to which a degraded image reflects the information present in a reference image. Its calculation for a given pair of images requires knowledge of the underlying distribution of input X and output Y, as well as their joint distribution, which in practice is not possible as only realizations of the distributions (images) are available. Approximating the distribution through the image histogram is commonly applied and provides a good solution e.g. when the goal is to maximize MI for the purpose of registration. However, it leads to a poor approximation of the true value of entropy, since the pixel values in an image have a strong local dependence and conditioning a pixel to its neighborhood drastically reduces the entropy. Ideally, one should calculate the conditional entropy of each pixel given an infinite neighborhood, as shown by Ignatenko *et al.*[8] In practice, a small neighborhood is sufficient for a reasonable approximation, if a Gaussian model is assumed for the dependence of a pixel on its neighbors. Unfortunately, even approximations using a small neighborhood lead to problems of very high dimensionality and thus computational cost.

It is possible to bypass this limitation if we consider another aspect of Shannon's theory. In the context of coding, MI gives the rate of information transfer through a communication channel. The maximum of this

rate is equal to the channel capacity, for which Shannon gave an elegant definition. For the case of a one-dimensional, zero-mean signal of bandwidth B, which is corrupted by independent additive white Gaussian noise, the maximum information capacity of the channel $C_{Shannon}$ can be written in the simple form:

$$C_{Shannon} = max\left\{H(Y) - H(Y|X)\right\} = B \cdot \log_2\left(1 + \left(\frac{S}{N}\right)^2\right), \tag{3}$$

where $\left(\frac{S}{N}\right)^2$ is the signal-to-noise ratio, and the maximum is over all power-constrained input densities. Here the channel bandwidth is measured in Hz and $C_{Shannon}$ is expressed in bits per second (bps).

Shannon's noisy channel coding theorem can be generalized for two-dimensional signals where both signal and noise are zero-mean and bandwidth-limited and the noise is additive, Gaussian and possibly colored. In this case, the information capacity (C_0) per unit area can be calculated as:

$$C_0 = \int_{-f_{Nx}}^{f_{Nx}} \int_{-f_{Ny}}^{f_{Ny}} \log_2\left(1 + \frac{P(f_x, f_y)}{N(f_x, f_y)}\right) df_x\, df_y, \tag{4}$$

where $P(f_x, f_y)$ and $N(f_x, f_y)$ are the signal and noise power spectra[†], respectively, and the integration takes place up to the Nyquist frequency $f_N = (f_{Nx}, f_{Ny})$. In this calculation, the zero-frequency components of the spectra are discarded since the information is contained in the difference between the signal and the background, corresponding with the zero-mean demand in Equation (3). The unit of the result is bits per pixel (bpp) or bits per square millimeters (b/mm^2), depending on the spatial frequency units. This information capacity expresses the maximum amount of information per unit area that can be transmitted for a given signal and noise power and it is upper-bounded by the entropy of the source producing the signal. In this sense, it can be considered as a measure of the *information content* of a specific image at a given noise level. The contrast of the image is reflected in the signal power spectrum, where the signal is defined as a modulation over the background. Loss of sharpness is also incorporated in the signal power spectrum, since it follows the transfer characteristics of the imaging system. In this way, sharpness, contrast and noise are all reflected in this expression, which generalizes our further experiments.

To calculate C_0 as defined in Equation (4), it is first necessary to separate noise from signal. In our *full-reference* scheme, the signal term is represented by the noiseless reference, which is in practice obtained by averaging a large sequence of still images in order to decrease the noise to a negligible level. This is different from assuming a perfect (uncorrupted) image, which is also perfectly sharp. In the case of independent additive noise, subtracting this reference from the noisy (test) image provides the noise term in the denominator. In radiography, however, the assumption of independent noise does not hold, as will be elaborated in the next section.

3.2 Noise in X-ray imaging

The dominating type of noise in X-ray images is photon noise, which follows a Poisson distribution with standard deviation σ equal to the square root of the number of detected photons, which in turn is equal to the mean signal value μ, so $\sigma = \sqrt{\mu}$. At the detector plane, the measured signal is proportional to the number of photons with a factor k. For most acquisition conditions, the large number of photons per pixel causes the photon noise to approximate a Gaussian distribution with variance proportional to the mean signal. To apply the Shannon theorem, however, the noise variance must be independent of the average signal.

To achieve signal-independence of the noise, we exploit the property that any invertible deterministic transformation on a signal has no effect on its information content, as expressed by the entropy of the signal[9]. It can be derived from the first part of Equation (2) that it also does not affect the value of the information capacity of a channel. Strictly speaking, this is only true for signals in the analog domain; in the case of X-ray images, we assume that the quantization is fine enough (10-14 bits per pixel) to approximately meet this demand.

[†]In this paper, the power spectra are calculated as the squared moduli of the Fourier spectra, as defined in stochastic signal theory.

For unprocessed images right after detection, it has been shown by Bartlett[10] that taking the square root as a transforming function results in transformed images with signal-independent noise variance. If σ_X, σ_Y are the standard deviations before and after the transformation, respectively, and $T(x)$ is the transforming function with derivative $T'(x)$, then using second-order Taylor expansions, we obtain $\sigma_Y^2 \approx (T'(\mu))^2 \cdot \sigma_X^2$, which in the case of $T(x) = \sqrt{x}$ leads to $\sigma_Y^2 \approx k/4$.

3.2.1 General method for variance stabilization of signal-dependent noise

After image acquisition at the detector, various operations are performed which affect both signal and noise. Consequently, the type of transformation that must be applied to achieve signal-independence of the noise depends on the transfer characteristics of the imaging chain up to the measuring point. Because many of the operations are non-linear and/or content dependent, we would like to calculate the appropriate transforming function using a "black box" approach, so with no knowledge of the specific transfer characteristics; we only measure the noise statistics at a given point in the imaging chain.

It has been shown by Arsenault and Denis[11] that signal-dependent noise can be transformed into signal-independent additive noise by means of a point transformation $T(x)$. This function depends on the pixel value x and is such that the transformed image $I' = T(I)$ is obtained by applying T on each pixel. For the case of a known relation $\sigma(\mu)$ between standard deviation and mean signal, and under the assumption that $\sigma << \mu$ (which generally holds even for low-dose images), it is shown that this transformation is given by the equation:

$$T(x) = K \cdot \int \frac{1}{\sigma(x)} dx, \tag{5}$$

and results in $\sigma(\mu) \approx K$ for all μ. The constant K determines the absolute value of σ, and will be considered unity in the following, as we are interested in the stabilization of standard deviation and not its absolute value. By applying this mapping, we will attempt to stabilize the noise standard deviation at any measuring point in the IP chain, even if the specific transfer functions up to that point are not known.

3.2.2 Noise statistics measurement in X-ray sequences

In order to determine the aforementioned transformation, the noise statistics need to be measured at any point in the imaging chain. The sample mean and sample variance can be measured in uniform areas of the image, where fluctuations are only due to noise. For doing this, an appropriate phantom (e.g. a step phantom) must be used. An example of this is shown in Figure 1(a), which shows an image of a step phantom after detection, gain control and white compression. In clinical phantoms, measuring the spatial noise statistics is more complex as it requires a separation between signal and noise variations. The implementation of the algorithms involved, e.g. as described by Aach *et al.*[12], requires significant manual tuning.

In our assessment scheme it is necessary to obtain a sequence of still images in order to create a noiseless reference; this implies that the current model does not incorporate object movement or the effect of system lag in the information content of images, but is rather designed for the quality assessment of still images. Because of this design constraint, it is also possible to measure noise statistics in the temporal instead of the spatial domain, which allows the use of general clinical phantoms as well. If the system is ergodic, so if the temporal statistics are equal to the spatial statistics, we can substitute measuring the statistics in uniform regions with measuring the statistics of each pixel along the temporal axis.

To examine the ergodicity of the system, we have performed both spatial and temporal statistics measurements on the step phantom of Figure 1(a). For the spatial statistics, the standard deviation was measured within the uniform regions of the phantom for each of the frames in the sequence. For N_{reg} number of regions and N_{fr} number of frames, the resulting number of points (mean-standard deviation pairs) is $N_{reg} \cdot N_{fr}$. The measured value for standard deviation was then corrected for the slow gradient along the horizontal axis found in X-ray images due to the heel effect. For the temporal statistics, the standard deviation of each pixel throughout the sequence was measured, so the number of points is $N_x \cdot N_y$, where N_x, N_y are the horizontal and vertical sizes of the image in pixels. The results of this comparison are shown in Figure 1(b), which shows a very small deviation ($< 1\%$) between the spatial and temporal statistics measurements. A flow diagram of the steps taken for the calculation of information capacity is depicted in Figure 2.

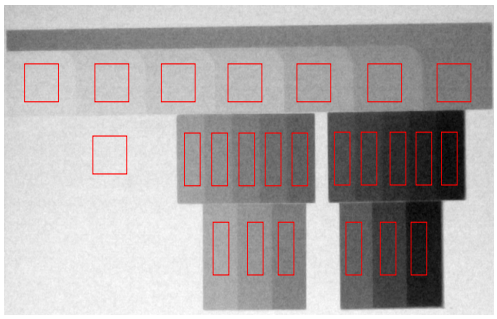

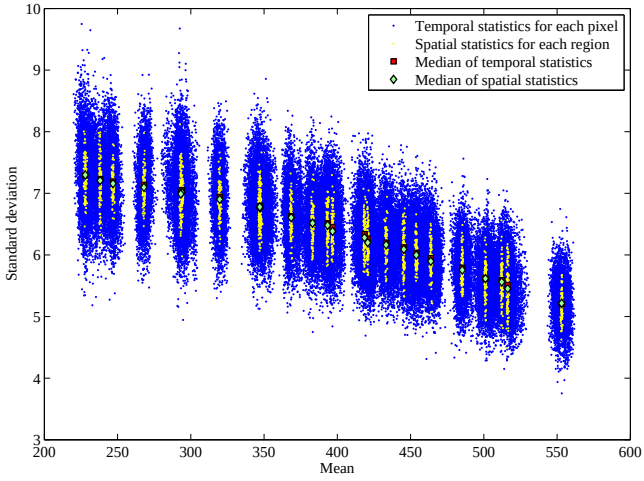

(a) (b)

Figure 1. Noise measurements. (a) Image of step phantom with uniform regions indicated by rectangles. (b) Comparison between standard deviation with respect to mean, measured spatially and temporally for the step phantom of (a) .

4. EXPERIMENTS AND IMPLEMENTATION

4.1 Image acquisition

A number of experiments were performed on the Allura Xper FD20 system to test the proposed method. The phantoms used were: the TO20 contrast-detail phantom of the University of Leeds[13], a standard Funk Type 38 phantom, a number of aluminium step phantoms with thicknesses between 0.5 mm and 12.5 mm (such as the one in Figure 1(a)) and an RSD RS-330 chest phantom.

In the case of technical (non-clinical) phantoms, the acquired images were corrected for the slow gradient due to the heel effect, as this is a dominant low-frequency component of the power spectrum while containing no true signal information. Perceptually, this slow gradient is not interpreted as information[14]. Although it is not within the scope of this work to include perceptual issues, we chose to perform this correction in order to measure the effect of signal variations only. For the chest phantom images, this was not necessary, as the signal spectrum in these images dominates over the low-frequency contribution of the heel effect.

System settings (tube current, voltage, pulse width) were varied between experiments, depending on the IQ parameter under consideration. The relation between tube current and noise variance is linear; varying the current with constant voltage and pulse width allows us to isolate the effect of noise. Sequences of 100 frames were acquired and temporal averaging of these sequences results in an SNR improvement of a factor of 10, which yields in a negligible amount of noise in the reference image.

To examine the effect of blurring separately, we chose to vary geometrical blurring by using two different focal spot sizes. The reason for examining geometrical blurring is because it affects only the sharpness of the resulting image; postsampling blur, on the other hand, also affects the noise, making comparisons more difficult. In the Allura Xper FD20, the nominal focal spot sizes are 0.4 mm for the small focus and 0.7 mm for the large focus. The tolerances for these values are described in IEC standard 60336[15], however, the exact focal spot size also varies with input power and usage time. For these two focal spot sizes, images of a detail phantom were made with increasing tube current at a fixed tube voltage, using the maximum source-imager distance (SID) of 120 cm and placing the phantom in the iso-center to stress the effect of magnification. The noise level and contrast for any given pair of images at the same tube current is identical; they differ only in sharpness. Figure 3 shows two images of a Funk 38 resolution phantom acquired with the two different focal spot sizes.

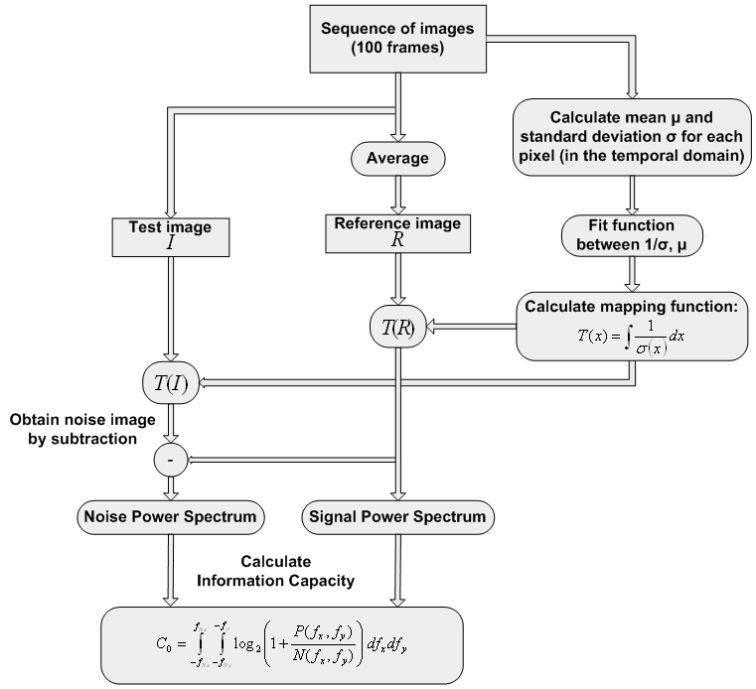

Figure 2. Flow diagram of calculation of C_0.

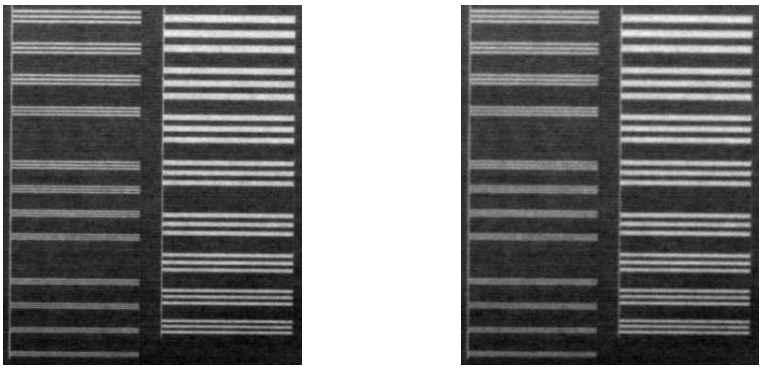

(a) (b)

Figure 3. Image of a type 38 Funk phantom. (a) Small focal spot. (b)Large focal spot. The difference in sharpness is visible in the left part of the image.

4.2 Variance stabilizing transformation

The transformation described in Section 3.2 is applied on a sequence of phantom images. Figure 4 shows the reference image of a chest phantom and the standard deviation, calculated for each pixel, before and after the transformation. Prior to the transformation, the difference in noise variance for regions of different average gray level is apparent (Figure 4(b)). After the transformation, it can be seen that the variance image appears more uniform, apart from the regions around sharp edges (Figure 4(c)). The instability around the edges is likely caused by minor registration errors (due to e.g. small vibrations of the table), which lead to fluctuations in the

measured temporal variance. The stabilization of standard deviation with respect to the mean can be seen in Figure 5, in which the statistics before and after transformation are shown.

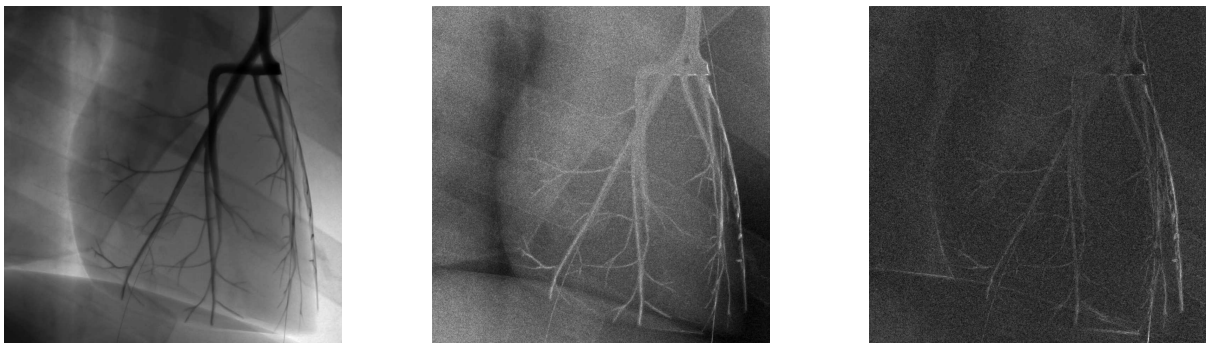

(a) (b) (c)

Figure 4. Result of noise stabilization. (a) Reference image of chest phantom. (b) Standard deviation for each pixel, measured along the temporal axis, before transformation. (c) Standard deviation after transformation (rescaled and shown in the same range as (b)).

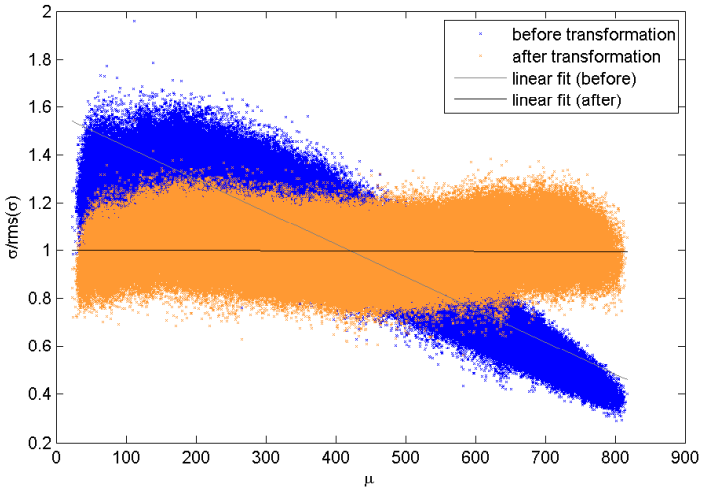

Figure 5. Scatter plot of standard deviation with respect to the mean for the chest phantom image of Figure 1(a), before and after transformation. The standard deviation is normalized by its rms value to allow comparison between the different ranges of the results. A straight line has been plotted through the scatter plots to show the overall flattening of σ with μ.

4.3 Effect of image processing

The next step is to attempt to extend this description throughout the various steps of the imaging chain.

As a first experiment, we study the effect of quantization by decreasing the number of representation levels. In this case, there are two types of noise degrading the image: quantization and quantum noise. For practical values of the bit depth (> 4 bpp), the quantization noise is approximately independent of the signal and of the

photon noise. Below these values, the quantization noise can no longer be considered signal-independent and tends to mask the photon noise. For the case of at least 5 bpp, the effect of the two noise sources on C_0 can be approximated as:

$$C_0 \approx \int_{-f_{Nx}}^{f_{Nx}} \int_{-f_{Ny}}^{f_{Ny}} \log_2 \left(1 + \frac{P(f_x, f_y)}{N_{ph}(f_x, f_y) + N_q(f_x, f_y)}\right) df_x \, df_y,$$

where N_{ph} and N_q are the power spectra of photon and quantization noise, respectively. In fact, the quantization noise distribution approximates a uniform, rather than a Gaussian, distribution, and our derivation of C_0 follows the reasoning presented in Huck *et al*[3]. To separate the calculation of the noise components, the photon noise is calculated between the unquantized reference and the unquantized test image, while the quantization error is obtained by subtracting the quantized reference from its original counterpart, as shown in Figure 6.

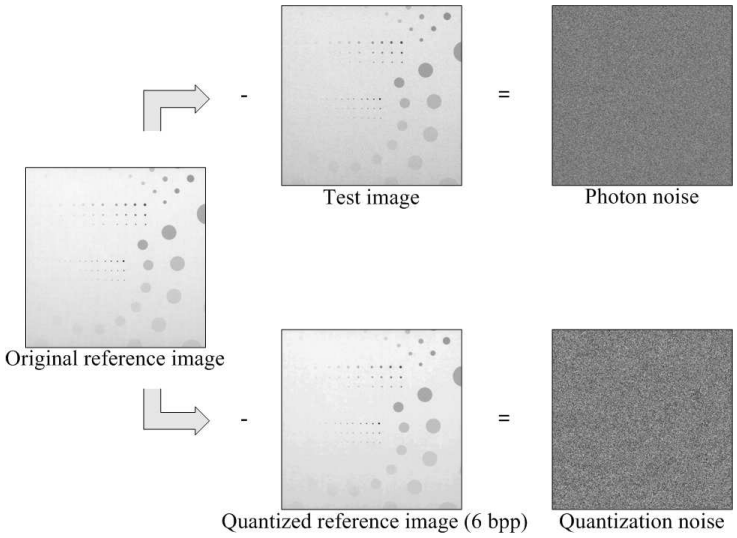

Figure 6. Separate calculation of photon noise (above) and quantization noise (below, for quantization at 6 bpp).

Next, we look into an example of a more advanced image-processing module, namely XRes™ of the Allura Xper FD20 system. This is a noise reduction and contrast enhancement module, implemented in a multiresolution scheme, which operates locally in the image, reducing noise in uniform areas while improving the contrast of structures[16]. To evaluate the IQ improvement due to XRes™ , all other image-processing operations were switched off. An example for a part of the chest phantom image of Figure 4(a) is shown in Figure 7[‡].

5. RESULTS

In this section we show some results for the information capacity of a number of phantom images.

Figure 8 shows the results for C_0 with respect to the tube current for the case of the two different focal spot sizes. The increase along the horizontal axis is due to reduction of noise with the tube current, while the improved sharpness of the smaller focal spot is reflected in the difference in measured information capacity between the two curves.

In Figure 9, the results for a varying number of representation levels is shown for different dose rates. This result is only reliable for values of a bit depth above 5 bpp, as mentioned in Section 4.3; below this, the masking effect of the quantization noise on photon noise causes an artificial increase in the value of C_0. Above this value, C_0 increases smoothly up to about 11 bpp, beyond which it shows no significant increase.

[‡]For better viewing of the differences please refer to the electronic version of this paper

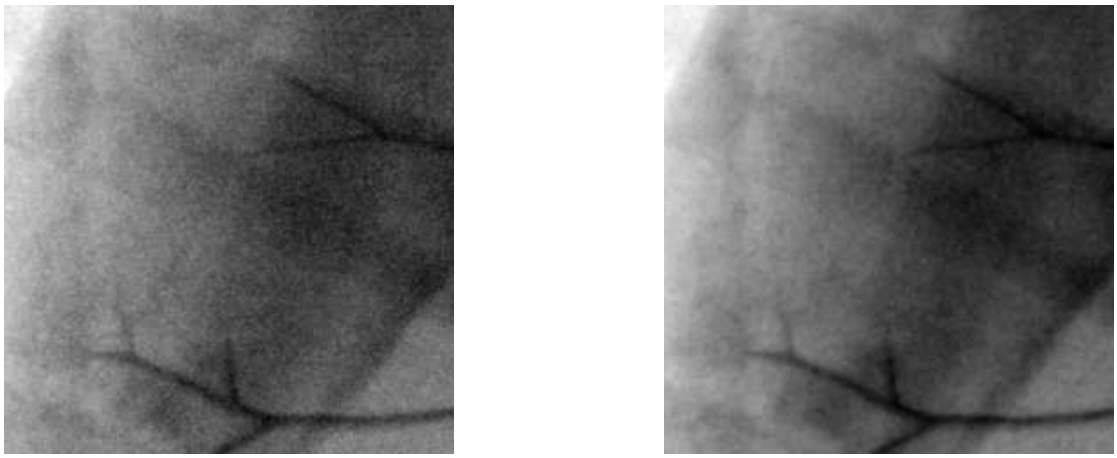

(a) (b)

Figure 7. Part of chest phantom image (a) before and (b) after XRes^{TM} .

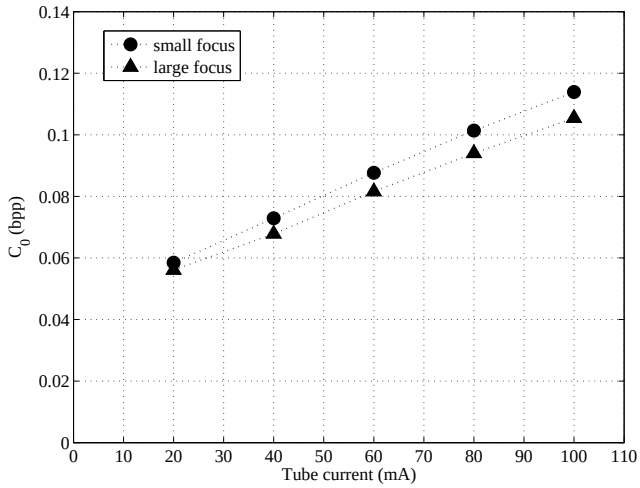

Figure 8. Information capacity for funk phantom of Figure 3 with increasing tube current, for small and large focal spot.

Figure 10 shows the improvement achieved with the XRes^{TM} module. The increase in C_0 mainly reflects the significant noise reduction; the direction-dependent and multiscale noise filtering avoids the blurring introduced by global filters. The benefits of local processing of image information are reflected in the results.

6. CONCLUSIONS

In this paper, we have applied Shannon's noisy channel coding theorem to a quality assessment of X-ray images. This assessment leads to a FOM which describes the information capacity of an image, assuming a sequence of still images is available. The image sequence is required to obtain a noiseless reference image by averaging the individual noisy images. For the derivation of this FOM, a pixel-wise transformation was described and proven to be successful in making the noise variance signal-independent, in compliance with the demands of Shannon's theorem. The method was then applied to phantom images obtained with different acquisition settings, and at different points within the imaging chain. In these experiments, the proposed information capacity metric corresponded well to the introduced variations.

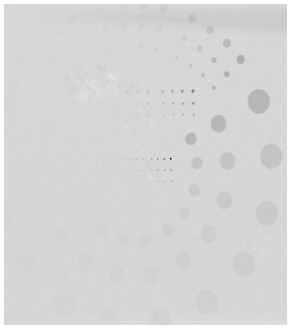

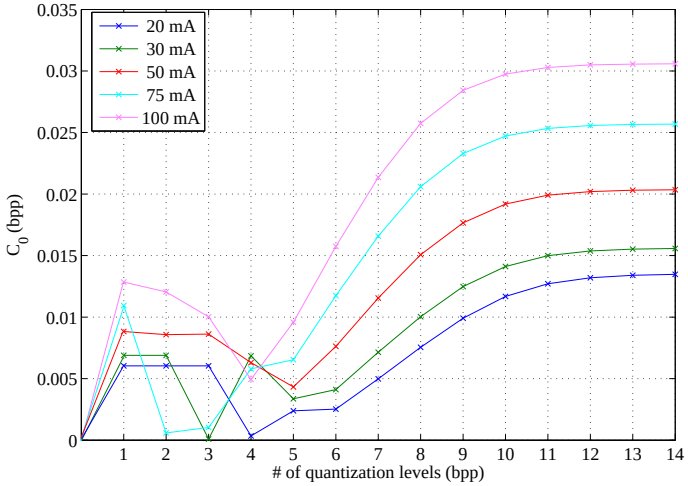

(a) (b)

Figure 9. (a) Contrast-detail phantom (b) Information capacity of (a) with respect to the number of quantization levels, for different tube currents.

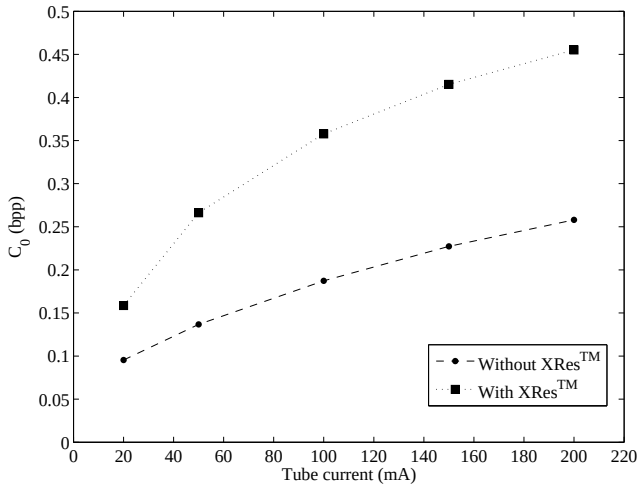

Figure 10. Information capacity of image of Figure 4(a) with and without processing with XRes^{TM} with respect to tube current.

The proposed FOM combines the effect of contrast, sharpness and noise. In this sense, its performance in describing overall image quality may be compared with that of measures from linear systems theory such as MTF for sharpness transfer and NPS for noise; such a comparison is within the scope of our future research. Furthermore, this approach can be applied for the evaluation of both the information transfer in X-ray systems as a function of dose, as well as the performance of image-processing algorithms. Such a description of image quality in the information domain may facilitate the study of the relation (and possible trade-offs) between dose and image processing.

REFERENCES

1. S. P. Awate and R. T. Whitaker, "Unsupervised, information-theoretic, adaptive image filtering for image restoration," *IEEE Trans. Pat. Anal. Mach. Intel.* **28**, pp. 364–376, 2006.
2. J. P. W. Pluim, J. B. A. Maintz, and M. A. Viergever, "Mutual information based registration of medical images: a survey," *IEEE Trans. Med. Im.* **22**, pp. 986–1004, 2003.
3. F. O. Huck, C. L. Fales, and Z. Rahman, *Visual Communication: An Information Theory Approach*, Kluwer Academic Publishers, Dordrecht, The Netherlands, 1997.
4. R. Wagner, D. Brown, and M. Pastel, "Application of information theory to the assessment of computed tomography," *Med. Ph.* **6**, pp. 83–94, 1979.
5. M. Fuderer, "The information content of MR images," *IEEE Trans. Med. Im.* **7**, pp. 368–380, 1988.
6. H. Sheikh, A. Bovik, and G. de Veciana, "An information fidelity criterion for image quality assessment using natural scene statistics," *IEEE Trans. Im. Proc.* **14**, pp. 2117–2128, 2005.
7. C. E. Shannon, "A mathematical theory of communication," *Bell Syst. Tech. J.* **27**, pp. 379–423, 1948.
8. T. Ignatenko, G. Schrijen, B. Skoric, P. T. Tuyls, and F. M. J. Willems, "Estimating the secrecy-rate of physical unclonable functions with the context-tree weighting methods," in *Proc. IEEE Int. Symp. on Information Theory*, pp. 449–503, 2006.
9. T. M. Cover and J. A. Thomas, *Elements of Information Theory*, John Wiley and Sons, New York, NY, 1991.
10. M. S. Bartlett, "The square root transformation in analysis of variance," *Suppl. J. R. Stat. Soc.* **3**, pp. 68–78, 1936.
11. H. H. Arsenault and M. Denis, "Integral expression for transforming signal-dependent noise into signal-independent noise," *Opt. Let.* **6**, pp. 210–212, 1981.
12. T. Aach, U. Schiebel, and G. Spekowius, "Digital image acquisition and processing in medical x-ray imaging," *J. Elec. Im.* **8**.
13. D. S. Evans, A. Mackenzie, C. P. Lawinki, and D. Smith, "Threshold contrast detail detectability curves for fluoroscopy and digital acquisition using modern image intensifier systems," *Br. J. Radiol.* **77**, pp. 751–758, 2004.
14. J. A. Ferwerda, S. N. Pattaniak, P. Shirley, and D. P. Greenberg, "A model for visual adaptation for realistic image synthesis," in *SIGGRAPH '96: Proc. 23rd annual conference on computer graphics and interactive techniques*, H. Rushmeier, ed.
15. ISO/IEC, "Medical electrical equipment - X-ray tube assemblies for medical diagnosis - Characteristics of focal spots - International standard 60336."
16. J. Y. Meuwly, J. P. Thiran, and F. Gudinchet, "Application of adaptive image processing tecnhique to real-time spatial compound ultrasound imaging improves image quality," *Inv. Radiol.* **38**, pp. 257–262, 2003.